Effective attraction between like-charged colloids in a two-dimensional plasma

Ning Ma,[1] S. M. Girvin,[1] and R. Rajaraman[2]

[1]*Department of Physics, Indiana University, Bloomington, Indiana 47405*
[2]*School of Physical Sciences, Jawaharlal Nehru University, New Delhi, 110067 India*

The existence of attractions between like-charged colloids immersed in ionic solution has been discovered in recent experiments. This phenomenon contradicts the predictions of Derjaguin-Landau-Verwey-Overbeek and indicates a failure of mean-field theory. We study a toy model based on a two-dimensional one-component plasma, which is exactly soluble at one particular coupling constant. We show that colloidal interaction results from a competition between ion-ion repulsion and longer ranged ion-void attraction.

I. INTRODUCTION

Recent experiments show convincingly the existence of attractions between like-charged colloids immersed in ionic solution, in particular in the vicinity of a glass wall or when the colloids are confined between glass walls [1,2]. This remarkable counterintuitive phenomenon is inconsistent with the well established theory of Derjaguin, Landau, Verwey, and Overbeek (DLVO) and has generated various theoretical interpretations.

It was shown [3] that counterion correlation forces, because of the long range of the electrostatic potentials, are usually not pairwise additive. Many-body effects [4] and Coulomb depletion forces [5] have been invoked to explain attractive forces between like-charged macroions. An exact demonstration [6] proved that the nonlinear Poisson-Boltzmann mean-field equation cannot give attractions in the case of Dirichlet boundary conditions. The argument was extended to a broader class of models [7] and boundary conditions [8]. Recently, there was a significant attempt based on nonequilibrium hydrodynamic effects [9].

In this paper, we solve a two-dimensional (2D) one-component plasma model exactly at a certain coupling constant following the method of Jancovici [10]. We have found a semianalytic method that extends the exact solution to the case in which colloidal particles are present. We treat the colloids in the plasma as empty regions (voids) from which the ions are excluded. The colloid may have fixed charge at its center. The analytic results obtained for small-sized colloids show that while the ion-ion repulsion, which varies as e^{-R^2} (R is the separation distance) in this particular 2D model, is strong at short distances, the ion-void attraction, which varies as $R^2 e^{-R^2}$, becomes dominant at large distances. The latter property is not normally found in conventional mean-field approximations, and must come from strong correlation effects. For large-sized colloids, we also have numerical results that qualitatively agree with the analytic ones. The present state of understanding of how to treat fluctuations beyond mean-field theory reliably is not very good despite the fact that this is an old problem [11–13]. Thus, our exact results may serve as a testing ground for more sophisticated approximation schemes. In addition, since this is a 2D model, the results are of interest in con-

nection with the problem of interactions among linear polyelectrolyte molecules [14].

In the sections that follow, we shall first review the plasma model in Sec. II. Then in Secs. III and IV we calculate the ion-ion and void-void interactions in the plasma system, respectively. Section V puts the above results together by treating the colloid as an empty region plus a fixed ion charge at the center. We have relegated the technical details as much as possible to the Appendixes.

II. THE PLASMA SYSTEM

We start by reviewing the exact solution for the one-component 2D plasma system [10]. Our approach is to map the classical plasma system into a quantum Hall system. Such an analogy allows one to describe the interacting ions in terms of noninteracting electrons occupying certain quantum obitals and subsequently use tools already developed. The advantage of this approach will become clearer later when we extend the same analogy to more complicated systems with fixed ion charges or/and empty regions present.

A. The quantum orbital language

The one-component 2D plasma system is composed of n simple ions embedded in a disk of uniform background charge. Each ion carries a charge of -1; the disk has a radius r and an areal charge density of ρ_0. Throughout this paper, we shall express all lengths in the unit of $\ell_0 = 1/\sqrt{\pi \rho_0}$. Thus, a unit circle contains unit amount of background charge, and the charge neutrality condition can be written simply as

$$n = r^2. \tag{2.1}$$

In two dimensions, it is convenient to use a complex number $z = x + iy$ (in units of ℓ_0) to represent the location of (x, y). Using z_i to denote the position of the ith ion, we can solve the 2D Poisson equation (in which the charges interact logarithmically rather than with the usual 3D $1/r$ interaction) [17] and find the total Coulomb potential energy of the system:

$$V = \frac{1}{2} \sum_{i=1}^{n} |z_i|^2 - \sum_{i<j}^{n} \ln|z_i - z_j|. \tag{2.2}$$

Here the first term describes the attractions between the ions and the background charge, and the second term represents the mutual repulsions among the ions themselves.

At inverse temperature $\beta \equiv 1/k_B T = 2$, the Boltzmann factor reads:

$$e^{-\beta V} = \exp\left(-\sum_{i=1}^{n} |z_i|^2\right) \left|\prod_{i<j}^{n} (z_i - z_j)\right|^2. \qquad (2.3)$$

Written in the above form, the Boltzmann factor can be identified as the square of the determinant of a matrix $\mathbf{M}$,

$$e^{-\beta V} = |\det \mathbf{M}|^2, \qquad (2.4)$$

with the matrix elements being the lowest Landau level (LLL) wave functions studied in connection with the quantum Hall effect [15]:

$$M_{ij} = \psi_i(z_j) \equiv \frac{z_j^{i-1}}{\sqrt{\pi \Gamma(i)}} e^{-|z_j|^2/2}. \qquad (2.5)$$

The above wave function describes an electron occupying the ith angular momentum orbital in the LLL. In this quantum language, $\det \mathbf{M}$ is a Slater determinant and represents the Laughlin wave function at filling factor $\nu = 1$, describing a fully filled Landau level. Thus, the complicated Coulomb interactions are replaced by a simple Slater determinant. The determinant representation of the Boltzmann factor was first noted by Jancovici [10] prior to the discovery of the quantum Hall effect. We recapitulate (and then extend) his argument in more modern language.

B. The partition function

Armed with this powerful quantum analogy, we proceed to calculate the partition function of the system, by integrating out all the ionic degrees of freedom:

$$Z = \prod_{i=1}^{n} \int dz_i e^{-\beta V}. \qquad (2.6)$$

This is nothing more than the norm of the Laughlin wave function, and hence can be computed exactly. Substituting Eq. (2.4) in Eq. (2.6) and expanding the determinant, we have

$$Z = \prod_{i=1}^{n} \int dz_i |\det \mathbf{M}|^2$$

$$= \prod_{i=1}^{n} \int dz_i \sum_{\{\mathcal{P}\}} \sum_{\{\mathcal{Q}\}} (-1)^{\mathcal{P}+\mathcal{Q}} \prod_{i=1}^{n} \bar{\psi}_{P_i}(z_i) \psi_{Q_i}(z_i), \qquad (2.7)$$

where $\mathcal{P}$ and $\mathcal{Q}$ are permutations of $\{1:n\}$ ($1:n$ is a shorthand notation for $1, 2, \ldots, n$) that come from the expansions of $\det \bar{\mathbf{M}}$ and $\det \mathbf{M}$, respectively. In Eq. (2.7), we have both summations and integrations which respectively represent the Coulomb interactions and the thermal averages. It is use-

ful at this point to postpone treating the Coulomb interactions until after the thermal averages are done. Thus, we switch the order of the summations and integrations in Eq. (2.7) so that

$$Z = \sum_{\{\mathcal{P}\}} \sum_{\{\mathcal{Q}\}} (-1)^{\mathcal{P}+\mathcal{Q}} \prod_{i=1}^{n} \int dz_i \bar{\psi}_{P_i}(z_i) \psi_{Q_i}(z_i)$$

$$\equiv \sum_{\{\mathcal{P}\}} \sum_{\{\mathcal{Q}\}} (-1)^{\mathcal{P}+\mathcal{Q}} \prod_{i=1}^{n} \langle P_i | Q_i \rangle, \qquad (2.8)$$

where $\langle i | j \rangle$ is the Dirac notation for the inner product of the ith and jth LLL orbitals. Notice that the summations over $\{\mathcal{Q}\}$ can be identified as a matrix determinant:

$$\sum_{\{\mathcal{Q}\}} (-1)^{\mathcal{P}+\mathcal{Q}} \prod_{i=1}^{n} \langle P_i | Q_i \rangle = \sum_{\{\mathcal{R}\}} (-1)^{\mathcal{R}} \prod_{i=1}^{n} \langle i | R_i \rangle = \det \mathbf{O}, \qquad (2.9)$$

where $\mathcal{R} \equiv \mathcal{Q} \circ \mathcal{P}^{-1}$ is the composite permutation of $\mathcal{Q}$ and $\mathcal{P}^{-1}$, and the *overlap matrix* $\mathbf{O}$ defined by

$$O_{ij} = \langle i | j \rangle \qquad (2.10)$$

is a matrix composed of LLL wave function inner products. Here, just as previously, the complicated Coulomb interactions are again replaced by a simple matrix determinant. Finally, we substitute Eq. (2.9) into Eq. (2.8) to obtain

$$Z = \sum_{\{\mathcal{P}\}} \det \mathbf{O} = n! \det \mathbf{O}. \qquad (2.11)$$

The immaterial factor of $n!$ will be dropped henceforth. Through the quantum analogy, the statistical problem is reduced to evaluating the overlap matrix $\mathbf{O}$ and its determinant. This is particularly simple in the present case; because of orthonormality we know that matrix $\mathbf{O}$ is an identity matrix.

C. The plasma edge

Near the plasma edge, physical properties are quite different from those in the bulk. This motivates us to study the boundary effects separately. For simplicity, we are going to be mainly interested in a *soft* boundary condition, which restricts the range of the ions' angular momenta rather than their positions. The ions can go anywhere in the complex plane; nevertheless, they are most likely to be found inside a disk with radius $r = \sqrt{n}$ because their angular momenta are bounded by n [recall that the lth LLL state has angular momentum of $(l-1)$ and peaks in a shell $\sqrt{l-1} < r < \sqrt{l}$]. The advantage of using this type of boundary condition is apparent: we can continue to use the same wave functions to describe the ions near the edge. What is implicitly assumed here is that the uniform background charge does not cease at the plasma edge; it extends to infinity. We also note that in the thermodynamic limit ($r \to \infty$) the circular plasma edge becomes locally flat.

One may also consider putting some ''surface'' charge on the plasma boundary. But, as indicated below, this effect can be absorbed in shifting the position of the boundary. We assume the surface charge, if any, does not fluctuate. Depending on its sign, the boundary charge either increases or decreases the number of available angular momentum channels. This is more or less equivalent to varying the radius r of the plasma disk in a system with neutral boundary. Hence, without loss of generality, we may assume boundaries are neutral.

Another type of plasma system we want to address in this paper is a plasma strip with two parallel edges separated by h. This can be realized in the thermodynamic limit by a system of ions with angular momenta ranging from $(r-h/2)^2$ to $(r+h/2)^2$. The double edged system thus differs from a single edged system *only* in the momentum range. To avoid redundancy, we shall use the single edged system as the example in our calculations. By changing the angular momentum limits, the results can easily be transferred to double edged systems.

III. FIXED ION CHARGES IN A PLASMA

In this section, we shall apply the same method to a slightly more complicated plasma system, with one or two ion charge(s) fixed at certain position(s). The resulting partition function is conventionally called the one- or two-body density function. The physical significance is twofold. First, we can learn from these density functions about how the ions are distributed and how two ions are correlated. More importantly, the fixed ion charges can be viewed as the limiting case of small-sized charged colloids. Thus, the results obtained in this section will provide us with many useful insights to the colloidal interactions.

A. The one-body density function

First we consider the one-body density function. We fix the position $z_1 = w$ and integrate out the remaining ionic degrees of freedom,

$$Z^{(1)} = \prod_{i=2}^{n} \int dz_i e^{-\beta V} \bigg|_{z_1=w}$$

$$= \prod_{i=2}^{n} \int dz_i |\det \mathbf{M}|^2 \bigg|_{z_1=w} = \sum_{\{\mathcal{P}\}} \sum_{\{\mathcal{Q}\}} (-1)^{\mathcal{P}+\mathcal{Q}}$$

$$\times \bar{\psi}_{P_1}(w) \psi_{Q_1}(w) \prod_{i=2}^{n} \langle P_i | Q_i \rangle. \tag{3.1}$$

The summations over P_1 and $\{\mathcal{Q}\}$ then reduce to a matrix determinant

$$\sum_{P_1} \sum_{\{\mathcal{Q}\}} (-1)^{\mathcal{P}+\mathcal{Q}} \bar{\psi}_{P_1}(w) \psi_{Q_1}(w) \prod_{i=2}^{n} \langle P_i | Q_i \rangle = -\det \mathbf{O}^{(1)}, \tag{3.2}$$

with the $(n+1) \times (n+1)$ matrix $\mathbf{O}^{(1)}$ defined by

$$\mathbf{O}^{(1)} \equiv \begin{bmatrix} \mathbf{O} & \Psi^{\dagger}(w) \\ \Psi(w) & 0 \end{bmatrix}. \tag{3.3}$$

Here, $\mathbf{O}$ (not to be confused with $\mathbf{O}^{(1)}$) is the $n \times n$ overlap matrix defined in Eq. (2.10); $\Psi \equiv (\psi_1, \psi_2, \ldots, \psi_n)$ is a row vector of LLL wave functions representing the fixed ion charge, and $\Psi^{\dagger}$ is its conjugate transpose. Finally, the remaining summations over $\{P_{i,(i=2:n)}\}$ in Eq. (3.1) just yield a trivial prefactor:

$$Z^{(1)} = \sum_{\{P_{i(i=2:n)}\}} -\det \mathbf{O}^{(1)} = -(n-1)! \det \mathbf{O}^{(1)}. \tag{3.4}$$

To evaluate the determinant of matrix $\mathbf{O}^{(1)}$, we apply Schur's theorem (discussed in detail in Appendix B) and find

$$Z^{(1)} = -\det \mathbf{O}^{(1)} = \det \mathbf{O} \det[\Psi(w)\mathbf{O}^{-1}\Psi^{\dagger}(w)]_{1 \times 1}$$

$$= \sum_{k=1}^{n} \psi_k(w) \bar{\psi}_k(w), \tag{3.5}$$

where we have used the fact that the overlap matrix $\mathbf{O}$ is an identity matrix. Using Eq. (A7), we convert the above series into translation coefficients (TCs) defined in Eq. (A6):

$$Z^{(1)} = \sum_{k=1}^{n} \psi_k(w) \bar{\psi}_k(w) = \frac{1}{\pi} \sum_{k=1}^{n} |T_{k1}(w)|^2. \tag{3.6}$$

Now that the partition function is written in the form of a TC sum, we may use the TC sum rules listed in Appendix A 2. We consider the following two cases.

If the fixed ion is in the bulk of the plasma ($w \ll r = \sqrt{n}$), we may take the limit $n \to \infty$ first and use TC sum rule (A14) to obtain

$$Z^{(1)} = \frac{1}{\pi}. \tag{3.7}$$

This tells us that deep in the bulk the ion density is constant and equal to the background charge density everywhere.

Near the plasma edge, we assume the boundary is located at $(r+h/2)$ and the fixed ion is located at $w = re^{i\theta}$, so that the ion is $h/2$ away from the boundary. In this case, we can use TC sum rule (A23) in Eq. (3.6) to obtain

$$Z^{(1)s} = \frac{1}{2\pi} \left[1 + \Phi\left(\frac{h}{\sqrt{2}}\right) \right]. \tag{3.8}$$

Here, the superscript s means a single edged system (in contrast to d, which means double edged system) and $\Phi(x)$ is the standard error function. As shown in Fig. 1, the ion density indeed drops from its bulk value to zero upon crossing the soft plasma boundary (at $h=0$).

B. The two-body density function

In calculating the one-body density function, we find that a fixed ion charge amounts to an additional row and column in the overlap matrix. This result can be generalized for sys-
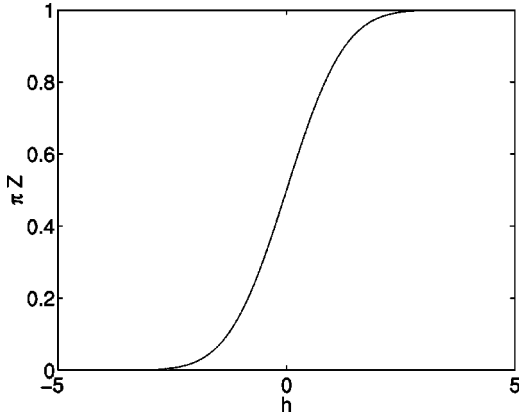
FIG. 1. The one-body density function near the plasma edge (length in units of ℓ_0).

tems with multiple fixed ion charges. In particular, we consider the two-body density function with $z_1 = w$ and $z_2 = \bar{w}$ fixed. The result is

$$Z^{(2)} = -\det \mathbf{O}^{(2)}, \qquad (3.9)$$

where $\mathbf{O}^{(2)}$ is an $(n+2) \times (n+2)$ matrix:

$$\mathbf{O}^{(2)} \equiv \begin{bmatrix} \mathbf{O} & \Psi^\dagger(w) & \Psi^\dagger(\bar{w}) \\ \Psi(w) & 0 & 0 \\ \Psi(\bar{w}) & 0 & 0 \end{bmatrix}. \qquad (3.10)$$

Similarly, using Schur's theorem and Eq. (A7), we can write the correlation function in terms of TC sums:

$$Z^{(2)} = \det \mathbf{O} \det \left(\begin{bmatrix} \Psi(w) \\ \Psi(\bar{w}) \end{bmatrix} \mathbf{O}^{-1} \begin{bmatrix} \Psi^\dagger(w) & \Psi^\dagger(\bar{w}) \end{bmatrix} \right)_{2 \times 2}$$

$$= \frac{1}{\pi^2} \left[\sum_{k=1}^n |T_{k1}(w)|^2 \right]^2 - \frac{1}{\pi^2} \left| \sum_{k=1}^n T_{k1}^2(w) \right|^2. \qquad (3.11)$$

In the bulk of the plasma ($w \ll r$), we assume $w = iR/2$ so that the two fixed ions are R apart. Inserting TC sum rules (A14) and (A15) into Eq. (3.11), and using Eq. (A9) for $T_{11}(iR)$, we obtain

$$Z^{(2)} = \frac{1}{\pi^2} [1 - |T_{11}(iR)|^2] = \frac{1}{\pi^2} (1 - e^{-R^2}). \qquad (3.12)$$

The above result tells us that the Coulomb repulsion between the two ion charges is heavily screened by the other ions and becomes short ranged. Its decay has a Gaussian form, which is much faster than the exponential form that DLVO theory predicts.

Near the plasma edge, we assume the boundary is located at $(r+h/2)$ and the fixed ions are located at $w = re^{i\theta}$ and $\bar{w}$, where $\theta \equiv R/2r$ so that the fixed ions are $h/2$ away from the edge and R apart from each other. Using TC sum rules (A23) and (A26) in Eq. (3.11), we obtain (for asymptotically large R)

$$Z^{(2)s} = \frac{1}{4\pi^2} \left\{ \left[1 + \Phi\left(\frac{h}{\sqrt{2}}\right) \right]^2 - \frac{2e^{-h^2}}{\pi R^2} \right\}. \qquad (3.13)$$

The above result shows that the ion-ion correlation function has a power law decay near the plasma edge. This is fundamentally different from the bulk behavior, and is due to the dipole moments induced by the sharp cutoff in angular momentum.

Finally, in the double edged system where the plasma edges are located at $(r \pm h/2)$, we may use TC sum rules (A30) and (A33) in Eq. (3.11) to obtain (for asymptotically large R)

$$Z^{(2)d} = \frac{1}{\pi^2} \left[\Phi^2\left(\frac{h}{\sqrt{2}}\right) - \frac{e^{-h^2}}{2\pi R^2} \sin^2(hR) \right]. \qquad (3.14)$$

Here, we find the correlation is not only long ranged, but oscillating with a period of $2\pi h^{-1}$ as well.

C. Divalent ions

A divalent ion can be viewed as composed of two simple ions occupying the same place. Here we want to calculate the two-body density function for a pair of divalent ions embedded in the monovalent plasma. Let us assume $z_1 = z_2 = w$ and $z_3 = z_4 = \bar{w}$ are fixed, where $w = iR/2$, so that the two divalent ions are R apart. Naively, one may follow Eq. (3.10) and write down an $(n+4) \times (n+4)$ matrix:

$$\tilde{\mathbf{O}}^{(4)} \equiv \begin{bmatrix} \mathbf{O} & \Psi^\dagger(z_1) & \Psi^\dagger(z_2) & \Psi^\dagger(z_3) & \Psi^\dagger(z_4) \\ \Psi(z_1) & 0 & 0 & 0 & 0 \\ \Psi(z_2) & 0 & 0 & 0 & 0 \\ \Psi(z_3) & 0 & 0 & 0 & 0 \\ \Psi(z_4) & 0 & 0 & 0 & 0 \end{bmatrix}. \qquad (3.15)$$

However, the matrix $\tilde{\mathbf{O}}^{(4)}$ defined above is singular because $z_1 = z_2$ (or $z_3 = z_4$). This singularity actually originates from the Boltzmann factor in Eq. (2.3), where we incorrectly include the self-interaction between z_1 and z_2 (or z_3 and z_4). To get around this problem, we must extract the singular factors from the matrix determinant. More precisely, we want to consider the following limits:

$$\det \mathbf{O}^{(4)} \equiv \lim_{z_2 \to z_1} \lim_{z_4 \to z_3} \frac{\det \tilde{\mathbf{O}}^{(4)}(z_1, z_2, z_3, z_4)}{|z_2 - z_1|^2 |z_4 - z_3|^2}. \qquad (3.16)$$

To construct matrix $\mathbf{O}^{(4)}$ from $\tilde{\mathbf{O}}^{(4)}$, we subtract $\Psi(z_1)$ in the $(n+1)$th row from $\Psi(z_2)$ in the $(n+2)$th row in Eq. (3.15). The resulting $(n+2)$th row then yields a factor of $(z_2 - z_1)$:

$$\lim_{z_2 \to z_1} [\Psi(z_2) - \Psi(z_1)] = (z_2 - z_1)\Psi'(z_1), \qquad (3.17)$$

where $\Psi' \equiv (\psi_1', \psi_2', \ldots, \psi_n')$, and ψ' is the first derivative of ψ. More precisely, following the usual procedure for the

Hilbert space of analytic functions [15,16], we take the derivative to act only on the analytic part of ψ and not on the Gaussian factor. The latter represents the interaction with the background charge and does not possess the self-interaction

singularity.

The factors of $(\bar{z}_2 - \bar{z}_1)$ and $|z_4 - z_3|^2$ can be extracted via similar procedures and we are left with a matrix that looks like

$$\mathbf{O}^{(4)} \equiv \begin{bmatrix} \mathbf{O} & \Psi^\dagger(w) & \Psi^{\dagger\prime}(w) & \Psi^\dagger(\bar{w}) & \Psi^{\dagger\prime}(\bar{w}) \\ \Psi(w) & 0 & 0 & 0 & 0 \\ \Psi'(w) & 0 & 0 & 0 & 0 \\ \Psi(\bar{w}) & 0 & 0 & 0 & 0 \\ \Psi'(\bar{w}) & 0 & 0 & 0 & 0 \end{bmatrix}. \tag{3.18}$$

Applying Schur's theorem and using various TC sum rules listed in Appendix 2, one finds

$$Z^{(4)} = -\det \mathbf{O}^{(4)}$$

$$= \frac{1}{\pi^4} \det \begin{bmatrix} 1 & 0 & e^{-R^2/2} & 0 \\ 0 & 1 & Re^{-R^2/2} & e^{-R^2/2} \\ e^{-R^2/2} & Re^{-R^2/2} & 1 & R \\ 0 & e^{-R^2/2} & R & 1+R^2 \end{bmatrix}$$

$$= \frac{1}{\pi^4} [(1 - e^{-R^2})^2 - R^4 e^{-R^2}]. \tag{3.19}$$

To compare the correlation functions of divalent ions and simple ions (in the bulk case), we plot Eqs. (3.12) and (3.19) in Fig. 2. Clearly, the divalent ion has a larger ''exchange hole'' near its origin.

IV. VOID COLLOIDS IN A PLASMA

In this section, we introduce two empty colloidal voids into the plasma system. We take the colloidal particle to be a
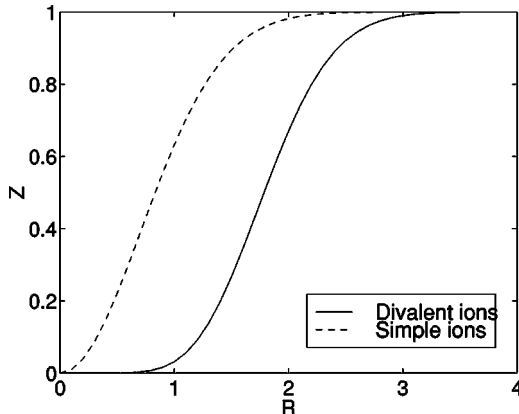

FIG. 2. Comparison between the two-body density functions for divalent ions (the solid line) and simple ions (the dashed line) in the bulk (length in units of ℓ_0).

circular disk with finite radius a, inside which ions are excluded. The presence of the voids clearly destroys the system's azimuthal symmetry. As a result, different angular momentum orbitals intersect, and the overlap matrix is generally not diagonal. It is the off-diagonal matrix elements that make the colloidal interactions nontrivial.

We shall fix the two voids at w and $\bar{w}$, respectively. Following Eq. (2.11), we can write down the partition function of the system as the determinant of the overlap matrix:

$$Z = \det \mathbf{O}. \tag{4.1}$$

Because the regions occupied by colloids are not accessible to the ions, their contribution to the overlap matrix should be excluded. Thus, in contrast to Eq. (2.10), here we have

$$O_{ij} = \langle i|j \rangle - \langle i|j \rangle_w - \langle i|j \rangle_{\bar{w}}, \tag{4.2}$$

where $\langle i|j \rangle_w$ means a partial inner product integrated over a circle with radius a centered at w. According to Eq. (A8), Eq. (4.2) can be explicitly evaluated as [18]

$$O_{ij} = \delta_{ij} - \left[\sum_{l=1}^{\infty} \gamma_l \bar{T}_{il}(w) T_{jl}(w) + \text{c.c.} \right], \tag{4.3}$$

where γ_l is the incomplete gamma function defined in Eq. (A4).

A. Analytic results

The off-diagonal matrix elements make the determinant in Eq. (4.1) difficult to analyze. However, if the colloidal size a is small, we can treat them perturbatively. From Eq. (A4) we know $\gamma_i \sim O(a^{2i})$ when $a \to 0$. Thus, to the lowest order in a, we can truncate the infinite summation in Eq. (4.3) at $l=1$:

$$O_{ij} \approx \delta_{ij} - \gamma_1 [\bar{T}_{i1}(w) T_{j1}(w) + T_{i1}(w) \bar{T}_{j1}(w)]. \tag{4.4}$$

If we define a $2 \times n$ matrix $\mathbf{J}$ as

$$\mathbf{J} \equiv \begin{bmatrix} T_{11}(w) & T_{21}(w) & \cdots & T_{n1}(w) \\ \bar{T}_{11}(w) & \bar{T}_{21}(w) & \cdots & \bar{T}_{n1}(w) \end{bmatrix}, \tag{4.5}$$

Eq. (4.4) may be rewritten in a matrix form:

$$\mathbf{O} = 1 - \mathbf{J}^\dagger \gamma_1 \mathbf{J}. \tag{4.6}$$

According to the corollary of Schur's theorem [see Appendix B, Eq. (B3)], we have

$$\det(1 - \mathbf{J}^\dagger \gamma_1 \mathbf{J})_{n \times n} = \det(1 - \mathbf{J} \gamma_1 \mathbf{J}^\dagger)_{2 \times 2}. \tag{4.7}$$

The determinant of a 2×2 matrix is easy to calculate and the result is (dropping terms with order higher than γ_1)

$$Z = \det \mathbf{O} \approx 1 - 2 \left(\sum_{k=1}^{n} |T_{k1}(w)|^2 \right) \gamma_1 = 1 - 2\gamma_1, \tag{4.8}$$

where we have used the TC sum rule (A14). Notice that the above (first order) result is R independent. This is no accident, because in order for the colloids to know the separation distance R, the Green's function needs to be integrated over both colloidal regions, which yields a term proportional to a^4, appearing in at least the second order in perturbation theory.

In the second order approximation, we must keep terms proportional to γ_1, γ_1^2, and γ_2. The procedure is quite similar to the above, and the result is

$$Z \approx 1 - 2 \left(\sum_{k=1}^{n} |T_{k1}(w)|^2 \right) \gamma_1 - 2 \left(\sum_{k=1}^{n} |T_{k2}(w)|^2 \right) \gamma_2$$
$$+ \left[\left(\sum_{k=1}^{n} |T_{k1}(w)|^2 \right)^2 - \left| \sum_{k=1}^{n} T_{k1}^2(w) \right|^2 \right] \gamma_1^2. \tag{4.9}$$

Compared to Eqs. (3.6) and (3.11), we find that the first and second order terms are, respectively, proportional to the one- and two-body density functions. Hence the colloidal void-void interaction does not differ very much from the ion-ion interaction we studied earlier in Sec. III.

In the plasma bulk, we assume $w = iR/2$ and use TC sum rules (A14) and (A15) in Eq. (4.9) to obtain

$$Z \approx 1 - 2\gamma_1 - 2\gamma_2 + (1 - e^{-R^2})\gamma_1^2; \tag{4.10}$$

near the plasma edge(s), we assume $w = re^{i\theta}$ ($\theta = R/2r$) and express Eq. (4.9) in terms of TC sum-rule results:

$$Z^{s,d} \approx 1 - 2A_{11}^{s,d}\gamma_1 - 2A_{22}^{s,d}\gamma_2 + [(A_{11}^{s,d})^2 - |B_{11}^{s,d}|^2]\gamma_1^2, \tag{4.11}$$

where the explicit forms for $A^{s,d}$ and $B^{s,d}$ for asymptotically large R can be found in Eqs. (A23), (A26), (A30), and (A33).

B. Numerical results

For large-sized colloids, the analytic results based on the small-a expansion may not be appropriate. We resort to numerical methods and use LU [19] factorization with partial pivoting to evaluate the matrix determinants. We find that (essentially) exact results can be obtained from relatively small matrix sizes.
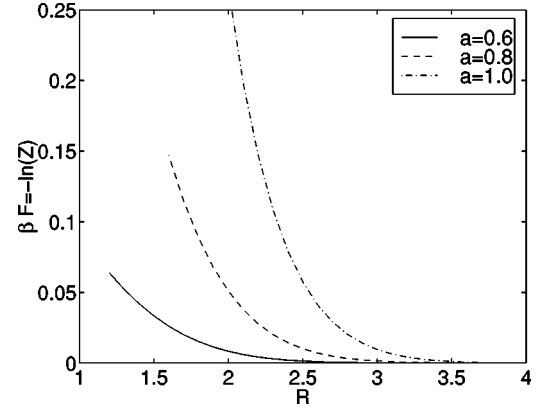

FIG. 3. Numerical results for the free energy of colloidal voids of radius a in the bulk of plasma separated by a distance R (length in units of ℓ_0).

For colloidal voids immersed in the bulk of the plasma, our numerical results are presented in Fig. 3. For a variety of sizes we studied, no attraction is found, confirming our analytic predictions.

Near the plasma edge(s), we find it more convenient to use square shaped colloids in numerical calculation. We assume the squares are of size $2a$, centered at $re^{i\theta}$ and $re^{-i\theta}$, respectively. [The plasma edge(s) are located at $(r \pm h/2)$.] Defining $\delta \equiv a/r$, we can calculate the overlap matrix in Eq. (4.2) as

$$O_{ij} = \delta_{ij} - \left[\int_{r-a}^{r+a} d\rho \int_{\theta-\delta}^{\theta+\delta} d\phi \frac{\rho^{i+j-1} e^{-\rho^2} e^{i(j-i)\phi}}{\pi \sqrt{\Gamma(i)\Gamma(j)}} + \text{c.c.} \right]. \tag{4.12}$$

In the limit $i \sim j \sim r^2 \to \infty$, the above integral can be evaluated asymptotically. The result is

$$O_{ij} \approx \delta_{ij} - C(\theta, \delta) \frac{\Gamma((i+j)/2)}{\sqrt{\Gamma(i)\Gamma(j)}} [\Phi(r_+) - \Phi(r_-)], \tag{4.13}$$

where,

$$r_\pm \equiv \frac{(r \pm a)^2 - (i+j)/2 + 1}{\sqrt{i+j-2}};$$

$$C(\theta, \delta) \equiv \frac{\cos[(i-j)\theta]\sin[(i-j)\delta]}{(i-j)\pi}$$

$[C(\theta, \delta)$ should be interpreted as δ/π in the case of $i = j$]. In practice, we keep increasing r until the numerical result becomes independent of r, which is found to occur approximately at $r = 60$. The results shown in Fig. 4 (for a single edged system) and Fig. 5 (for a double edged system) are computed using $r = 100$. In both figures, when the colloidal voids are far away from the edge(s) ($h = 6.0$), the curves are similar to those in Fig. 3, namely, the repulsive interaction has a Gaussian decay. As the colloids become closer to the
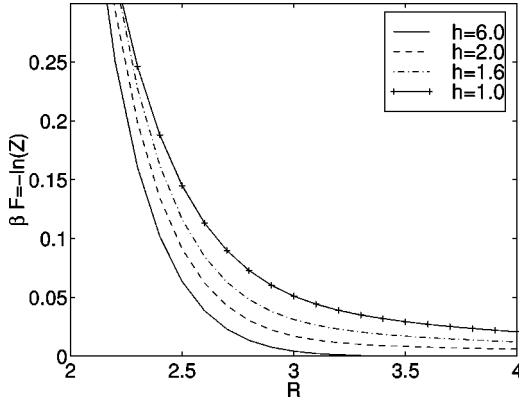
FIG. 4. Numerical results for the free energy of empty colloids of radius $a=1.0$ and located a distance $h/2$ away from a single plasma edge as a function of their separation R (length in units of ℓ_0).

plasma edge(s) (smaller h), the repulsion starts to develop a long tail, in agreement with our analytic results.

V. CHARGED COLLOIDS IN A PLASMA

We now consider charged colloids in the plasma. In the simplest case, the charged colloid is taken to be an empty disk plus a fixed ion charge at the center. The ion-ion interaction and void-void interaction have been studied in Secs. III and IV, respectively; both are repulsive. However, as we shall see in this section, the ion-void interaction is usually attractive, and has a longer range. The competition between the repulsion and attraction results in a richer behavior for the charged colloidal interactions.

Following Eqs. (3.9) and (3.10), we have the partition function as follows:

$$Z^{(2)} = -\det \mathbf{O}^{(2)}, \tag{5.1}$$

$$\mathbf{O}^{(2)} \equiv \begin{bmatrix} \mathbf{O} & \Psi^\dagger(w) & \Psi^\dagger(\bar{w}) \\ \Psi(w) & 0 & 0 \\ \Psi(\bar{w}) & 0 & 0 \end{bmatrix}, \tag{5.2}$$
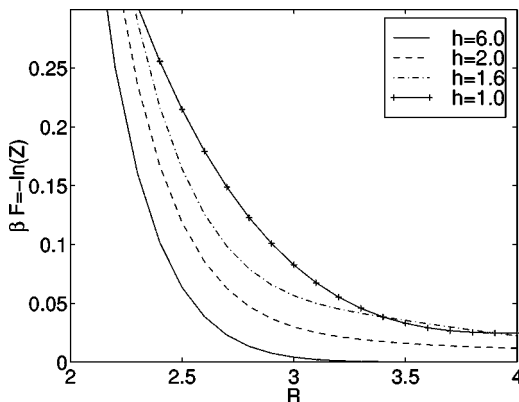

FIG. 5. Numerical results for the free energy of empty colloids of radius $a=1.0$ separated by a distance R in a plasma strip of width h (length in units of ℓ_0).

where $\Psi \equiv (\psi_1, \psi_2, \ldots, \psi_n)$ is a row vector representing the fixed ion charge at the colloidal center; the $n \times n$ overlap matrix $\mathbf{O}$, according to Eq. (4.3), is nondiagonal:

$$O_{ij} = \delta_{ij} - \left[\sum_{l=1}^\infty \gamma_l \bar{T}_{il}(w) T_{jl}(w) + \text{c.c.} \right]. \tag{5.3}$$

A. Analytic results

If the colloidal size a is small, we can obtain an analytic expression. One may truncate the infinite series in Eq. (5.3) at $l=1$:

$$O_{ij} \approx \delta_{ij} - \gamma_1 [\bar{T}_{i1}(w) T_{j1}(w) + T_{i1}(w) \bar{T}_{j1}(w)]. \tag{5.4}$$

However, we notice that the $(n+1)$th and $(n+2)$th rows of matrix $\mathbf{O}^{(2)}$ in Eq. (5.2) can be written as

$$O^{(2)}_{(n+1)j} = \psi_j(w) = \frac{T_{j1}(w)}{\sqrt{\pi}}, \tag{5.5}$$

$$O^{(2)}_{(n+2)j} = \bar{\psi}_j(w) = \frac{\bar{T}_{j1}(w)}{\sqrt{\pi}}. \tag{5.6}$$

If we multiply Eq. (5.5) by $\sqrt{\pi} \gamma_1 \bar{T}_{i1}(w)$, multiply Eq. (5.6) by $\sqrt{\pi} \gamma_1 T_{i1}(w)$, and add them together to the ith row, the off-diagonal part of O_{ij} in Eq. (5.4) is canceled completely. Thus the final answer does not contain γ_1. This is true even if we do not make any truncations in Eq. (5.4). Physically, it originates from the fact that the first angular momentum channel is occupied by the fixed ion, so it is not accessible to the free ions. Another way of saying this is that the fixed ion serves as a ''Laughlin quasihole'' in the quantum electron system.

To obtain a nontrivial result, we consider the second angular momentum channel $l=2$:

$$O_{ij} \approx \delta_{ij} - \gamma_2 [\bar{T}_{i2}(w) T_{j2}(w) + T_{i2}(w) \bar{T}_{j2}(w)]. \tag{5.7}$$

Applying Schur's theorem, we have

$$Z^{(2)} = \det \mathbf{O} \det \left(\begin{bmatrix} \Psi(w) \\ \Psi(\bar{w}) \end{bmatrix} \mathbf{O}^{-1} [\Psi^\dagger(w) \quad \Psi^\dagger(\bar{w})] \right)_{2 \times 2}$$

$$\equiv Z_1 Z_2. \tag{5.8}$$

We first concentrate on the second factor Z_2. It describes the two fixed ions (represented by wave functions Ψ and $\Psi^\dagger$) interacting through the plasma medium (represented by matrix $\mathbf{O}^{-1}$). For small γ_2, the matrix $\mathbf{O}^{-1}$ can be approximated by

$$O^{-1}_{ij} \approx \delta_{ij} + \gamma_2 [\bar{T}_{i2}(w) T_{j2}(w) + T_{i2}(w) \bar{T}_{j2}(w)], \tag{5.9}$$

and Z_2 can be calculated to be [suppressing the (w) arguments]

$$Z_2 \approx \left[\left(\sum_{k=1}^{n} |T_{k1}|^2 \right)^2 - \left| \sum_{k=1}^{n} T_{k1}^2 \right|^2 \right] + 2\gamma_2 \left[\left(\sum_{k=1}^{n} |T_{k1}|^2 \right) \right.$$

$$\times \left| \sum_{k=1}^{n} T_{k1} T_{k2} \right|^2 + \left(\sum_{k=1}^{n} |T_{k1}|^2 \right) \left| \sum_{k=1}^{n} \bar{T}_{k1} T_{k2} \right|^2$$

$$- \left(\sum_{k=1}^{n} \bar{T}_{k1}^2 \right) \left(\sum_{k=1}^{n} T_{k1} \bar{T}_{k2} \right) \left(\sum_{k=1}^{n} T_{k1} T_{k2} \right) - \left(\sum_{k=1}^{n} T_{k1}^2 \right)$$

$$\left. \times \left(\sum_{k=1}^{n} \bar{T}_{k1} T_{k2} \right) \left(\sum_{k=1}^{n} \bar{T}_{k1} \bar{T}_{k2} \right) \right]. \tag{5.10}$$

We can interpret the above result by thinking of the colloidal voids as a perturbation to the plasma system plus fixed ions. The first square bracket in Eq. (5.10) is the result for the unperturbed system, namely, the ion-ion interaction via the plasma medium. It is precisely the two-body density function we obtained in Eq. (3.11). The second square bracket in Eq. (5.10) is the first order correction, namely, a fixed ion on one site interacting with the colloidal void on the *other* site. This ion-void interaction is usually found to be attractive, and since it involves higher order TC sums, its range is longer than that of the ion-ion repulsion (see results below). So far, we have missed another first order effect, namely, the fixed ion interacting with the colloidal void on the *same* site. The excess background charge underneath the void should reduce the effective ionic charge somehow. It turns out that this renormalization effect is captured precisely by the first factor Z_1 in Eq. (5.8):

$$Z_1 = \det \mathbf{O} \approx 1 - 2 \sum_{k=1}^{n} |T_{k2}|^2 \gamma_2. \tag{5.11}$$

In the bulk plasma, we assume $w = iR/2$ and use TC sum rules (A14) and (A15) to obtain

$$Z^{(2)} \approx (1 - 2\gamma_2)(1 - e^{-R^2}) + 2R^2 e^{-R^2} \gamma_2. \tag{5.12}$$

In the above equation, the first term is the renormalized ion-ion repulsion and the second term is the ion-void attraction. The attraction is proportional to $R^2 e^{-R^2}$, which has a longer range than the repulsion. This feature is not found in mean-field approximations, and thus must be caused by the strong correlation effects. Notice that the void-void repulsion and the renormalization of the ion-void attraction are both of second order, so they do not appear in Eq. (5.12). The repulsion and attraction respectively dominate the short distance and long distance behavior, and the minimum free energy $\beta F = -\ln Z^{(2)}$ occurs where the first derivative vanishes:

$$\frac{dZ^{(2)}(R^*)}{dR} = 0 \quad \text{or} \quad R^* = \sqrt{\frac{1}{2\gamma_2}}. \tag{5.13}$$

Figure 6 plots the calculated free energy vs R for various values of a. Note that, when γ_2 is small ($a = 0.6$), Eq. (5.13) predicts that the location of the free energy minimum is far
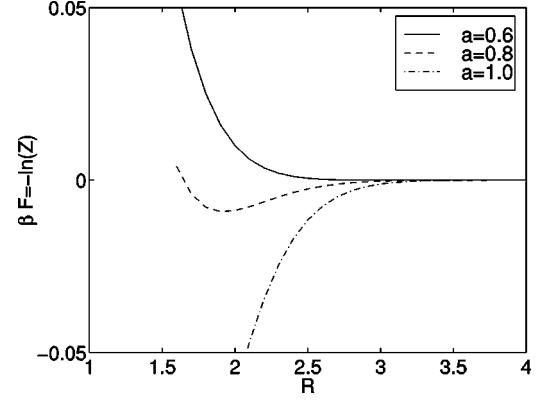

FIG. 6. Analytic results for the free energy vs separation distance R of singly charged colloids in the bulk of the plasma (length in units of ℓ_0).

away from the origin, in which case the attraction is strongly suppressed by the decaying factor e^{-R^2}, thus becoming virtually invisible.

Near the plasma edge, we use TC sum rules (A23) through (A27) to obtain (for asymptotically large R)

$$Z^{(2)s} \approx \left[(A_{11}^s)^2 - \frac{e^{-h^2}}{2\pi R^2} \right]$$

$$+ 2\gamma_2 \left[\frac{(A_{11}^s h^2 + A_{22}^s) e^{-h^2} - (2h/\sqrt{2\pi}) e^{-3h^2/2}}{2\pi R^2} \right.$$

$$+ A_{11}^s \left(\frac{e^{-h^2}}{\sqrt{2\pi}} - A_{11}^s A_{22}^s \right) \right]. \tag{5.14}$$

Similarly, for the double edged system, we use TC sum rules (A30) through (A34) to obtain

$$Z^{(2)d} \approx \left[(A_{11}^d)^2 - \frac{e^{-h^2}}{2\pi R^2} \sin^2(hR) \right]$$

$$+ 2\gamma_2 \left\{ \frac{[A_{11}^d h^2 \cos^2(hR) + A_{22}^d \sin^2(hR)] e^{-h^2}}{2\pi R^2} \right.$$

$$\left. - (A_{11}^d)^2 A_{22}^d \right\}. \tag{5.15}$$

B. Numerical results

Our numerical results for charged colloids in the bulk case are plotted in Fig. 7. When a is small ($a = 0.6 - 0.8$) the numerical results agree very well with the analytic ones presented in Fig. 6. However, when a is large ($a = 1.0$), the two differ significantly in that the numerical free energy has an additional secondary maximum. This peak reflects the even longer ranged, second order effects that are not accounted for in the analytic studies.

We also tried putting double ion charges at the center of each colloid. This case is very similar to the divalent ions
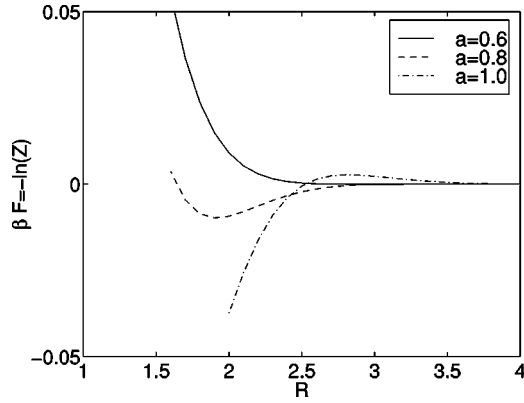
FIG. 7. Numerical results for the free energy vs separation distance R of singly charged colloids of radius a in the bulk of the plasma (length in units of ℓ_0).

FIG. 9. Numerical results for the free energy vs separation distance R of singly charged colloids near a single plasma edge; case I, $a=0.8$ (length in units of ℓ_0).

that are studied in Sec. III C. Our numerical results are presented in Fig. 8, where the colloidal sizes are chosen to be $\sqrt{2}$ times as large as those in Fig. 7, so that the two figures are comparable. We see that the qualitative behavior is very similar. The attraction minimum stays further out.

Near the plasma edge, we use squares to represent colloidal particles as we did in Sec. IV B. The numerical results for two different sizes of colloids are presented in Fig. 9 and Fig. 10. In case I ($a=0.8$, Fig. 9), when the colloids are far away from the edge ($h=5.0$) they repel; as they come closer to the edge ($h=2.3$) they start to attract each other within a certain range ($R<2.25$), but beyond that range they still repel; at a particular point ($h=1.5$), the range of the attraction seems to extend to infinity; finally, when they are too close to the edge ($h=0.8$), due to insufficient screening, a long range repulsion is found. In case II ($a=0.9$, Fig. 10), the colloids are larger in size and attract each other even in the bulk ($h=5.0$); the attraction becomes deeper ($h=2.0$) and longer ranged ($h=1.3$) as the colloids move toward the edge.

Figure 11 shows the free energy of colloids in a double edged system. When the two boundaries are widely separated ($h=5.0$), the colloids repel; as the separation decreases, the free energy develops a long oscillating tail.
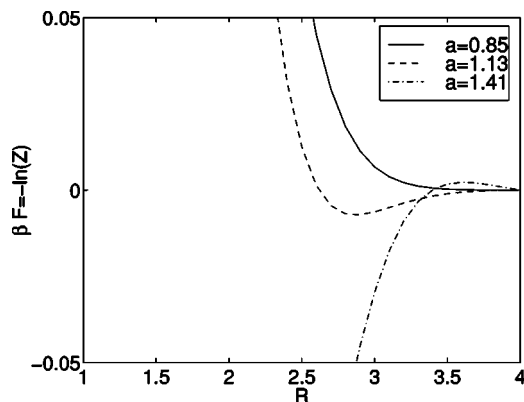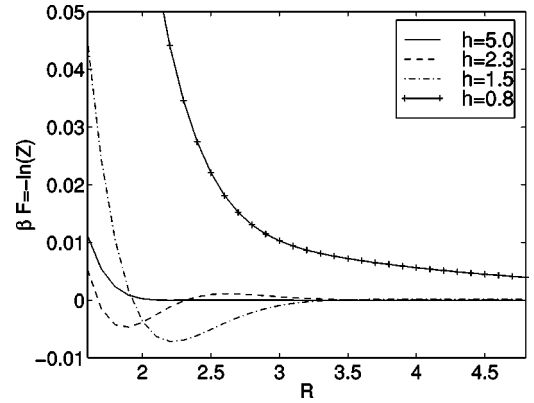
These results are consistent with the analytic results. Note that the oscillation "wavelength," according to Eq. (5.15), is set by the strip width h, and is independent of the size a of the colloids. This conclusion is confirmed by Fig. 12.

Finally, Fig. 13 shows the results for doubly charged colloids near a single plasma edge. They are qualitatively similar to those shown in Fig. 10.

C. Where does the colloid stay?

To better understand the charged colloidal interactions, especially near the plasma edge, it is instructive to learn where they prefer to stay in the plasma. We put a charged colloid at $w=re^{i\theta}$, which is $h/2$ away from the plasma edge at $(r+h/2)$, and calculate the partition function to be

$$Z^{(1)s}=-\det \mathbf{O}^{(1)}, \qquad (5.16)$$

$$\mathbf{O}^{(1)}=\begin{bmatrix} \mathbf{O} & \Psi^{\dagger}(w) \\ \Psi(w) & 0 \end{bmatrix}, \qquad (5.17)$$

where the $n\times n$ overlap matrix $\mathbf{O}$ is

FIG. 8. Numerical results for the free energy vs separation distance R of doubly charged colloids of radius a in the bulk of the plasma (length in units of ℓ_0).
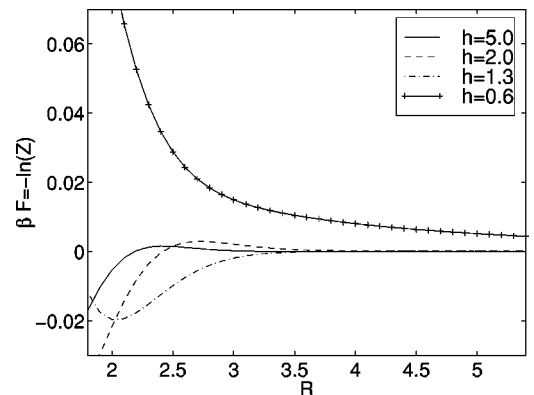

FIG. 10. Numerical results for the free energy vs separation distance R of singly charged colloids near a single plasma edge; case II, $a=0.9$ (length in units of ℓ_0).
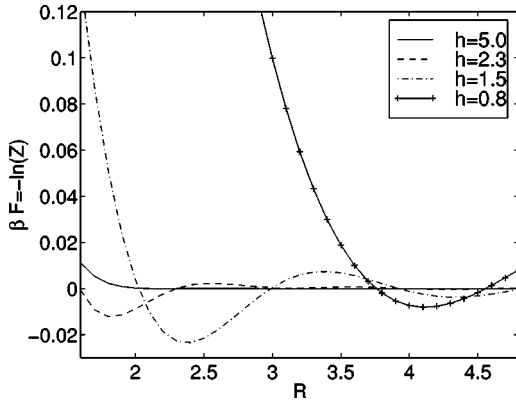
FIG. 11. Numerical results for the free energy vs separation distance R of singly charged colloids near double plasma edges; $a = 0.8$ (length in units of ℓ_0).

$$O_{ij} = \delta_{ij} - \sum_{l=1}^{\infty} \gamma_l \bar{T}_{il}(w) T_{jl}(w). \qquad (5.18)$$

It can be shown that the first angular momentum channel is blocked by the fixed ion charge so that the final answer does not depend on γ_1. For small a, we truncate the infinite summation in Eq. (5.18) at $l=2$ and use Schur's theorem to find

$$Z^{(1)s} \approx \left[1 - \sum_{i=1}^{n} |T_{i2}|^2 \gamma_2 \right] \left[\sum_{i=1}^{n} |T_{i1}|^2 + \left| \sum_{i=1}^{n} \bar{T}_{i1} T_{i2} \right|^2 \gamma_2 \right]$$

$$= A_{11}^s + \left(\frac{e^{-h^2}}{2\pi} - A_{11}^s A_{22}^s \right) \gamma_2. \qquad (5.19)$$

Figure 14 shows the numerical results obtained for a square charged colloid. We plot the free energy βF as a function of h for three different sized squares. In all cases, we find the colloid is attracted to a free energy minimum near the plasma edge (at $h=0$). For $h<0$, the free energy quickly blows up. This tells us that the colloid prefers not to leave from the plasma edge, because its fixed charge is attracted by the background charge and prefers to be in the
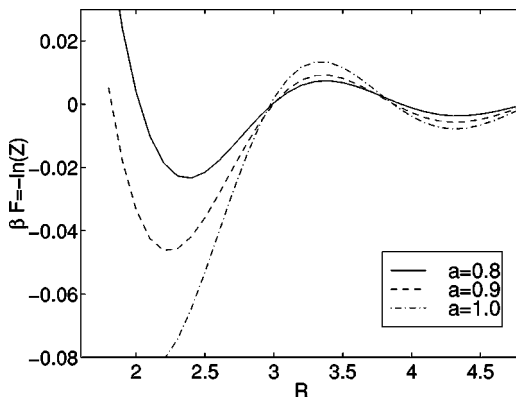

FIG. 12. Numerical results for the free energy vs separation distance R of singly charged colloids near double plasma edges; $h = 1.5$ (length in units of ℓ_0).
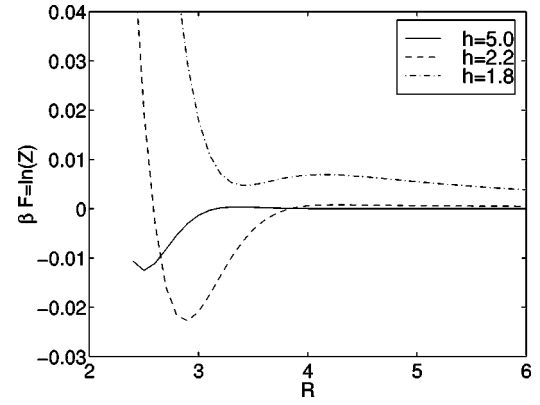

FIG. 13. Numerical results for the free energy vs separation distance R of doubly charged colloids near a single plasma edge; $a = 1.2$ (length in units of ℓ_0).

lowest available angular momentum channel. The optimal distance h^* is in the range in which attraction between colloids occurs.

VI. SUMMARY

In this paper, we considered a strongly coupled ($\beta=2$) 2D one-component plasma model and calculated the effective interaction between two colloids both in the bulk and near boundaries. Our calculations show that the interaction between colloids results in a competition among the ion-ion and void-void repulsions and the ion-void attraction. While it is somewhat difficult to assign a clear and simple physical mechanism to the net attraction, the model clearly contains both excluded volume effects analogous to those that produce attraction in hard sphere systems and also strong nonlinear (and fluctuating non-mean-field) screening of the long range Coulomb forces. Our (essentially exact) numerical results also show that proximity to the boundary of the plasma enhances the strength and range of the attraction. This is presumably due to softer fluctuation modes available near the edge of the incompressible plasma.

In this paper, we have assumed a logarithmic potential among the ions. In [17], we argued that this is not entirely unfaithful to the real physical system. The fact that the
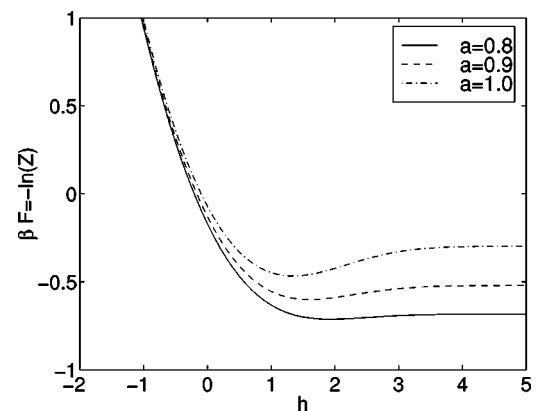

FIG. 14. Numerical results for the free energy for one singly charged colloid near a single plasma edge (length in units of ℓ_0).

plasma has one component rather than two is a more serious limitation which we hope to remedy in the future. Although our model is oversimplified, the exact results provide useful insights into the problem, and can serve as a testing ground for approximation schemes currently in use.

APPENDIX A: PROPERTIES OF LOWEST LANDAU LEVEL WAVE FUNCTIONS

A convenient formulation of quantum mechanics within the subspace of the lowest Landau level was developed by Girvin and Jach [15,16]. Here, we follow their formalism and summarize some important properties that are frequently used throughout the paper.

1. Orthonormality and completeness

The ith LLL wave function is defined as

$$\psi_i(z) = \frac{1}{\sqrt{\pi \Gamma(i)}} z^{i-1} e^{-|z|^2/2}. \tag{A1}$$

These LLL wave functions are orthonormal:

$$\langle i|j\rangle = \int dz\, \bar\psi_i(z) \psi_j(z) = \delta_{ij}. \tag{A2}$$

Sometimes, we want to calculate a partial inner product (the overlap integrated over part of the entire plane), and the result is generally not diagonal. However, if the integration region has azimuthal symmetry, the conservation of angular momentum guarantees an exception. As an example, let us take the region to be a circle with radius a centered at the origin (denoted by the subscript),

$$\langle i|j\rangle_0 = \int_0^a \rho\, d\rho \int_0^{2\pi} d\phi\, \frac{\rho^{i+j-2} e^{-\rho^2} e^{i(j-i)\phi}}{\pi\sqrt{\Gamma(i)\Gamma(j)}} = \delta_{ij}\gamma_i, \tag{A3}$$

where the incomplete gamma function γ_i is defined as

$$\gamma_i \equiv \frac{1}{\Gamma(i)} \int_0^{a^2} du\, e^{-u} u^{i-1} = 1 - e^{-a^2}\left(\sum_{k=0}^{i-1} \frac{a^{2k}}{k!}\right). \tag{A4}$$

Notice that in the limit $a\to 0$ $\gamma_i \sim O(a^{2i})$.

From Eq. (A1), it is clear that any wave function in the LLL can be written in the form

$$\psi(z) = f(z) e^{-|z|^2/2}, \tag{A5}$$

where $f(z)$ is an analytic function. Thus the subspace spanned by the LLL wave functions is isomorphic to the Hilbert space of analytic functions [15,16]. An example is the wave function $\psi_i(z)$ with its argument translated by a vector w:

$$e^{(\bar z w - z\bar w)/2}\psi_i(z+w) = \sum_{j=1}^\infty T_{ij}(w)\psi_j(z). \tag{A6}$$

Here, the extra pure phase factor in front of $\psi_i(z+w)$ is needed to cancel the additional nonanalytic part generated by the translation, so as to retain the translated wave function within the LLL.

2. Translation coefficients

The linear coefficients T_{ij} defined in Eq. (A6) are termed *translation coefficients*. Setting $z=0$ in Eq. (A6), we find

$$\psi_i(w) = \sum_{j=1}^\infty T_{ij}(w)\psi_j(0) = \frac{T_{i1}(w)}{\sqrt{\pi}}. \tag{A7}$$

Thus the LLL basis functions are just special cases of TCs. Another useful application of the TC is to calculate the partial inner product on a circle with radius a centered at $w \neq 0$ (denoted by the subscript):

$$\langle i|j\rangle_w = \int_{|z|<a} dz\, \bar\psi_i(z+w)\psi_j(z+w)$$

$$= \int_{|z|<a} dz \sum_{k,l} \bar T_{ik}(w)\bar\psi_k(z)\psi_l(z)T_{jl}(w)$$

$$= \sum_{k,l} \bar T_{ik}(w)\langle k|l\rangle_0 T_{jl}(w) = \sum_{l=1}^\infty \gamma_l \bar T_{il}(w)T_{jl}(w). \tag{A8}$$

The TCs can be evaluated explicitly. We multiply by $\bar\psi_k(z)$ on both sides Eq. (A6), and integrate z over the entire plane. On the right hand side, this picks out one particular T_{ik} from the summation because of the orthonormality:

$$T_{ik}(w) = \int dz\, e^{(\bar z w - z\bar w)/2}\bar\psi_k(z)\psi_i(z+w)$$

$$= \frac{e^{-|w|^2/2}}{\pi\sqrt{\Gamma(i)\Gamma(k)}} \int dz\, e^{-|z|^2 - z\bar w}\bar z^{k-1}(z+w)^{i-1}$$

$$= \frac{e^{-|w|^2/2}}{\pi\sqrt{\Gamma(i)\Gamma(k)}} \int dz\, e^{-|z|^2}\left[\sum_{t=0}^\infty \frac{(-\bar w)^t z^t}{t!}\right]\bar z^{k-1}$$

$$\times \left[\sum_{s=1}^i C_{s-1}^{i-1} z^{s-1} w^{i-s}\right]$$

$$= \sqrt{\Gamma(i)\Gamma(k)}(-1)^k \hat w^{i-k} e^{-|w|^2/2}$$

$$\times \sum_{s=1}^{\min(i,k)} \frac{(-1)^s |w|^{i+k-2s}}{\Gamma(s)(i-s)!(k-s)!}, \tag{A9}$$

where, in the third equation, we used Taylor and binomial expansions, and in the fourth equation we used orthonormality (A2). Equation (A9) immediately tells that the TCs have the following inversion symmetry:

$$T_{ij}(w) = \bar{T}_{ji}(-w) = T_{ji}(-\bar{w}). \tag{A10}$$

Another important property of the TC arises when one composes two successive translations:

$$T_{ij}(w_1+w_2) = e^{(\bar{w}_1 w_2 - w_1 \bar{w}_2)/2} \sum_{k=1}^{\infty} T_{ik}(w_1)T_{kj}(w_2). \tag{A11}$$

On using Eq. (A10), this becomes

$$T_{ij}(w_1+w_2) = e^{(\bar{w}_1 w_2 - w_1 \bar{w}_2)/2} \sum_{k=1}^{\infty} \bar{T}_{ki}(-w_1)T_{kj}(w_2) \tag{A12}$$

$$= e^{(\bar{w}_1 w_2 - w_1 \bar{w}_2)/2} \sum_{k=1}^{\infty} T_{ki}(-\bar{w}_1)T_{kj}(w_2). \tag{A13}$$

As a simple application, we set $-w_1 = w_2 = w$ in Eq. (A12):

$$\lim_{n\to\infty} \sum_{k=1}^{n} \bar{T}_{ki}(w)T_{kj}(w) = T_{ij}(0) = \delta_{ij}, \tag{A14}$$

or set $w_1 = w_2 = iR/2$ in Eq. (A13):

$$\lim_{n\to\infty} \sum_{k=1}^{n} T_{ki}\left(\frac{iR}{2}\right)T_{kj}\left(\frac{iR}{2}\right) = T_{ij}(iR). \tag{A15}$$

Note that if we interpret T_{ij} as the matrix elements of **T**, then Eq. (A14) has a simple matrix form,

$$\mathbf{T}^{\dagger}(w)\mathbf{T}(w) = 1, \tag{A16}$$

showing that matrix **T** is unitary. In the same matrix notation, Eq. (A10) is rewritten as

$$\mathbf{T}^{\dagger}(w) = \mathbf{T}(-w) \tag{A17}$$

which along with Eq. (A16) makes sense since $\mathbf{T}(-w)$ should be the inverse of $\mathbf{T}(w)$.

Equations (A14) and (A15) are examples of TC sum rules. They are frequently used in analyzing the bulk plasma. Near the edge, we often encounter TC summations of a different type:

$$A_{ij}^s \equiv \lim_{r\to\infty} \sum_{k=1}^{(r+h/2)^2} \bar{T}_{ki}(re^{i\theta})T_{kj}(re^{i\theta}), \tag{A18}$$

$$B_{ij}^s \equiv \lim_{r\to\infty} \sum_{k=1}^{(r+h/2)^2} T_{ki}(re^{i\theta})T_{kj}(re^{i\theta}). \tag{A19}$$

Here, the superscript s denotes the single edged system and $\theta \equiv R/2r$. The difference between the bulk TC sum and edge

TC sum is the following. Treated as a perturbation, colloids in the bulk mainly perturb the low angular momentum channels. Such a perturbation has a discrete characteristic, namely, only a small number of channels are strongly affected. Colloids near the boundary, on the other hand, perturb the high angular momentum channels. The perturbation has a continuum nature, namely, there are a large number of channels ($r^2 - hr < k < r^2 + hr$) that are weakly affected. As a result, the evaluation of the edge TC sum inevitably requires one to convert the discrete summation into a continuum integral. For example, let us calculate A_{11}^s:

$$A_{11}^s = \lim_{r\to\infty} \sum_{k=1}^{(r+h/2)^2} \frac{r^{2k-2}}{\Gamma(k)} e^{-r^2}$$

$$\approx \lim_{r\to\infty} \int_0^{r^2+hr} \frac{dx}{\sqrt{2\pi x}} e^{2x\ln r + x - x\ln x - r^2}, \tag{A20}$$

where we have defined $x \equiv k-1$ and used Stirling's asymptotic formula

$$\Gamma(x+1) \approx \sqrt{2\pi x}\, e^{-x+x\ln x}. \tag{A21}$$

The integal in Eq. (A20) can be evaluated using the saddle point approximation, in which one expands the exponent near its minimum at $x = r^2$ up to the second order:

$$A_{11}^s \approx \lim_{r\to\infty} \int_0^{r^2+hr} \frac{dx}{\sqrt{2\pi r}} e^{-(x-r^2)^2/2r^2}. \tag{A22}$$

Substituting $y \equiv (x-r^2)/r$, one finds

$$A_{11}^s = \int_{-\infty}^{h} \frac{dy}{\sqrt{2\pi}} e^{-y^2/2} = \frac{1}{2}\left[1 + \Phi\left(\frac{h}{\sqrt{2}}\right)\right], \tag{A23}$$

where $\Phi(x)$ is the standard error function. Other TC sum rules can be obtained through quite similar procedures. We omit the tedious derivations and simply list the results below:

$$A_{22}^s = \frac{1}{2}\left[1 + \Phi\left(\frac{h}{\sqrt{2}}\right) - \frac{he^{-h^2/2}}{\sqrt{2\pi}}\right], \tag{A24}$$

$$A_{12}^s = \frac{e^{-h^2/2}}{\sqrt{2\pi}}, \tag{A25}$$

$$B_{11}^s = \frac{e^{-h^2/2}}{\sqrt{2\pi R}} e^{i(hR-\pi/2)}, \tag{A26}$$

$$B_{12}^s = \frac{he^{-h^2/2}}{\sqrt{2\pi R}} e^{i(hR-\pi/2)}. \tag{A27}$$

Note that the above results are correct only asymptotically for $R\to\infty$ ($R \equiv 2r\theta$).

In a double edged system, we encounter the same type of TC summation, except that the lower limit is changed from $k=1$ to $k=(r-h/2)^2$:

$$A_{ij}^d \equiv \lim_{r \to \infty} \sum_{k=(r-h/2)^2}^{(r+h/2)^2} \bar{T}_{ki}(re^{i\theta}) T_{kj}(re^{i\theta}), \quad (A28)$$

$$B_{ij}^d \equiv \lim_{r \to \infty} \sum_{k=(r-h/2)^2}^{(r+h/2)^2} T_{ki}(re^{i\theta}) T_{kj}(re^{i\theta}). \quad (A29)$$

Correspondingly, we have (the superscript d denotes double edges)

$$A_{11}^d = \Phi\left(\frac{h}{\sqrt{2}}\right), \quad (A30)$$

$$A_{22}^d = \Phi\left(\frac{h}{\sqrt{2}}\right) - \frac{h e^{-h^2/2}}{\sqrt{2\pi}}, \quad (A31)$$

$$A_{12}^d = 0, \quad (A32)$$

$$B_{11}^d = \frac{e^{-h^2/2}}{\sqrt{2\pi R}} \sin(hR) e^{i(hR - \pi/2)}, \quad (A33)$$

$$B_{12}^d = \frac{h e^{-h^2/2}}{\sqrt{2\pi R}} \cos(hR) e^{i(hR - \pi/2)}. \quad (A34)$$

APPENDIX B: SCHUR'S THEOREM

For any four matrices $\mathbf{A}_{r \times r}$, $\mathbf{B}_{r \times s}$, $\mathbf{C}_{s \times r}$, and $\mathbf{D}_{s \times s}$, if $\mathbf{A}$ is not singular, Schur's theorem states

$$\det \begin{bmatrix} \mathbf{A} & \mathbf{B} \\ \mathbf{C} & \mathbf{D} \end{bmatrix} = \det \mathbf{A} \det(\mathbf{D} - \mathbf{C}\mathbf{A}^{-1}\mathbf{B}). \quad (B1)$$

The proof is straightforward. We consider the following matrix identity:

$$\begin{bmatrix} 1_{r \times r} & 0_{r \times s} \\ -\mathbf{C}\mathbf{A}^{-1} & 1_{s \times s} \end{bmatrix} \begin{bmatrix} \mathbf{A} & \mathbf{B} \\ \mathbf{C} & \mathbf{D} \end{bmatrix} = \begin{bmatrix} \mathbf{A} & \mathbf{B} \\ 0_{s \times r} & \mathbf{D} - \mathbf{C}\mathbf{A}^{-1}\mathbf{B} \end{bmatrix}. \quad (B2)$$

Taking the determinant of both sides of Eq. (B2), Eq. (B1) follows immediately.

Schur's theorem has a very useful corollary: for any matrices $\mathbf{J}_{r \times s}$ and $\mathbf{K}_{s \times r}$, one has

$$\det(1 - \mathbf{J}\mathbf{K})_{r \times r} = \det(1 - \mathbf{K}\mathbf{J})_{s \times s}. \quad (B3)$$

We can prove this by a very similar method. First we consider

$$\begin{bmatrix} 1_{r \times r} & -\mathbf{J} \\ 0_{s \times r} & 1_{s \times s} \end{bmatrix} \begin{bmatrix} 1_{r \times r} & \mathbf{J} \\ \mathbf{K} & 1_{s \times s} \end{bmatrix} = \begin{bmatrix} (1 - \mathbf{J}\mathbf{K})_{r \times r} & 0_{r \times s} \\ \mathbf{K} & 1_{s \times s} \end{bmatrix}, \quad (B4)$$

which tells us that

$$\det \begin{bmatrix} 1_{r \times r} & \mathbf{J} \\ \mathbf{K} & 1_{s \times s} \end{bmatrix} = \det(1 - \mathbf{J}\mathbf{K})_{r \times r}; \quad (B5)$$

on the other hand, if we consider

$$\begin{bmatrix} 1_{r \times r} & 0_{r \times s} \\ -\mathbf{K} & 1_{s \times s} \end{bmatrix} \begin{bmatrix} 1_{r \times r} & \mathbf{J} \\ \mathbf{K} & 1_{s \times s} \end{bmatrix} = \begin{bmatrix} 1_{r \times r} & \mathbf{J} \\ 0_{s \times r} & 1 - \mathbf{K}\mathbf{J} \end{bmatrix}, \quad (B6)$$

we obtain

$$\det \begin{bmatrix} 1_{r \times r} & \mathbf{J} \\ \mathbf{K} & 1_{s \times s} \end{bmatrix} = \det(1 - \mathbf{K}\mathbf{J})_{s \times s}. \quad (B7)$$

A combination of Eqs. (B5) and (B7) results in Eq. (B3). Letting $\mathbf{J} = \gamma_1 \mathbf{K}^\dagger$ in Eq. (B3), we obtain Eq. (4.7).

[1] G. M. Kepler and S. Fraden, Phys. Rev. Lett. **73**, 356 (1994).

[2] J. C. Crocker and D. G. Grier, Phys. Rev. Lett. **77**, 1897 (1996); A. M. Larsen and D. G. Grier, Nature (London) **385**, 230 (1997); D. G. Grier, *ibid.* **393**, 621 (1998).

[3] R. Podgornik and V. A. Parsegian, Phys. Rev. Lett. **80**, 1560 (1998).

[4] K. S. Schmitz, Langmuir **13**, 5849 (1998).

[5] E. Allahyarov, I. D'Amico, and H. Löwen, Phys. Rev. Lett. **81**, 1334 (1998).

[6] J. C. Neu, Phys. Rev. Lett. **82**, 1072 (1999).

[7] E. Trizac and J. L. Raimbault, e-print cond-mat/9909420.

[8] J. E. Sader and D. Y. Chan, J. Colloid Interface Sci. **213**, 268 (1999).

[9] T. M. Squires and M. P. Brenner, e-print cond-mat/0003195; E. R. Dufresne, T. M. Squires, M. P. Brenner, and D. G. Grier, e-print cond-mat/0003314.

[10] B. Jancovici, Phys. Rev. Lett. **46**, 386 (1981); J. Stat. Phys. **28**, 43 (1982); **29**, 263 (1982).

[11] R. P. Sear, e-print cond-mat/0002249.

[12] R. R. Netz and H. Orland, Eur. Phys. J. E **1**, 67 (2000); **1**, 203 (2000); Eur. Phys. J. D **8**, 145 (2000); Europhys. Lett. **45**, 726 (1999); Phys. Rev. E **60**, 3174 (1999); e-print cond-mat/9902220; e-print cond-mat/9902085, e-print cond-mat/9807009.

[13] L. S. Brown and L. G. Yaffe, e-print physics/9911055.

[14] B.-Y. Ha and A. J. Liu, in *Physical Chemistry of Polyelectrolytes*, edited by T. Radeva (Marcel Dekker, New York, in press); Phys. Rev. E **58**, 6281 (1998); **60**, 803 (1999).

[15] S. M. Girvin, in *Topological Aspects of Low Dimensional Systems*, Les Houches Lectures session LXIX (1998), edited by A. Comtet, J. Jolicoeur, S. Ouvry, and F. David (Springer-Verlag, Berlin/Les Editions Physique, Paris, 1999).

[16] S. M. Girvin and T. Jach, Phys. Rev. B **29**, 5617 (1984).

[17] In using a logarithmic potential, we are not being entirely un-

faithful to the physical system even though the microscopic Coulomb potential in quasi-2D systems is really $1/r$. As in the real experiment, we consider a point charge in a thin layer of water (with dielectric constant of about 70–80) sandwiched between glass plates of a much smaller dielectric constant of about 5–8. Then the electric lines of force due to the point charge will bend and try to stay in the electrolyte medium. This makes the electrostatics quasi-two-dimensional and brings the effective interaction closer to $\log(r)$.

[18] In a matrix notation, Eq. (4.3) can be written as $\mathbf{O}=1-[\mathbf{T}(w)\mathbf{G}\mathbf{T}^{\dagger}(w)+\mathbf{T}(\bar{w})\mathbf{G}\mathbf{T}^{\dagger}(\bar{w})]$, where $G_{ij}\equiv\delta_{ij}\gamma_{i}$. Using this, the free energy is given by

$$\beta F = -\ln \det \mathbf{O} = -\operatorname{tr}\ln\{1-[\mathbf{T}(w)\mathbf{G}\mathbf{T}^{\dagger}(w)+\mathbf{T}(\bar{w})\mathbf{G}\mathbf{T}^{\dagger}(\bar{w})]\}$$

$$= \sum_{k=1}^{\infty}\frac{1}{k}\operatorname{tr}[\mathbf{T}(w)\mathbf{G}\mathbf{T}^{\dagger}(w)+\mathbf{T}(\bar{w})\mathbf{G}\mathbf{T}^{\dagger}(\bar{w})]^{k} = \sum_{k=1}^{\infty}\frac{2}{k}\operatorname{tr}\mathbf{G}^{k}$$

$$+ F(w) = 2\beta F_{0} + \beta F(w),$$

where $\beta F_{0} \equiv -\ln \det(1-\mathbf{G})$ represents the free energy of each individual void, and $F(w)$ can be viewed as the interaction potential.

[19] W. H. Press, B. P. Flannery, S. A. Teukolsky, and W. T. Vetterling, *Numerical Recipes: The Art of Scientific Computing* (Cambridge University Press, Cambridge, 1986), p. 31.